SEISMIC RETROFIT OF RC BUILDINGS WITH VISCOUS DAMPERS AND ELASTIC STEEL FRAMES INCLUDING EFFECT OF COMPOSITE BEHAVIOR

Panumas SAINGAM[*], *Fatih SUTCU*[**] *Yuki TERAZAWA*[***],
Oguz C. CELIK[****] *and Toru TAKEUCHI*[*****]

This study proposes an alternative type of seismic retrofitting method for reinforced concrete (RC) buildings with a combination of viscous dampers and elastic steel frames, designed using an equivalent linearization approach. Within the scope of the study, the effect of composite behavior between the RC and closed steel frames is also considered as a key factor to reduce the demand of viscous dampers. A four-story RC school building is examined, and the proposed retrofit design method is validated using nonlinear response history analyses. The analysis results suggest that the proposed retrofit method can control maximum story drift ratio close to the design target. In addition, residual story drift ratios of the retrofitted buildings are substantially reduced. These results imply that both structural and nonstructural damage could be effectively mitigated in the retrofitted buildings using the proposed method that enhances self-centering properties.

Keywords **:** *Seismic retrofit, Viscous damper, RC buildings, Elastic steel frame, Composite behavior, Equivalent linearization*

1. INTRODUCTION

Over the past centuries, many reinforced concrete (RC) buildings were seriously damaged or collapsed during devastating earthquakes. Potential reasons for such heavy damage or collapses were reported from insufficient lateral force resistance, stiffness, ductility, or energy dissipation capacity. For example, Thailand has historically been considered to have a low seismic hazard risk, and the majority of existing buildings were not originally designed with adequate seismic resistance. However, as reported in [1-2], after the Mae Lao earthquake struck on the 15th, May 2014, that caused extensive damage to older buildings, much of the damage was observed in RC structures. Many public RC buildings, such as schools and hospitals, were seriously damaged by the earthquake. Similarly, significant damage was observed in many existing RC buildings reported in the post-earthquake survey reports in several other seismically vulnerable countries [3-7]. These reports have proven that retrofitting of these buildings with efficient methods is an urgent matter.

Conventional retrofit methods used to retrofit RC buildings by improving the lateral force resistance include wrapping RC columns with carbon fiber reinforced polymers (CFRP) [8-9], adding RC shear walls [10-11], or adding conventional (i.e. buckling) steel braces of several kinds and configurations [12-15]. On the other hand, innovative seismic retrofit methods to improve the seismic performance of a RC building such as adding energy-dissipation devices (dampers) are also available. Seismic retrofit of a RC building using dampers is experimentally proven to increase the energy dissipation capacity of the building [16-17].

Fluid viscous dampers (FVDs) and viscoelastic dampers are known to be effective in increasing the energy dissipation capacity of building structures [18-25]. Several studies proposed a displacement-based design method for designing structures with passive energy dissipation devices [26-30]. In order to simplify the design procedure, previous studies [31-32] proposed buckling-restrained braces (BRBs) retrofit design method for RC buildings without the need for iteration based on the equivalent linearization approach [33]. This procedure is named as constant drift (CD) method.

In this study, the CD method is extended to a seismic retrofit of RC buildings using FVDs implemented with an elastic steel frame (SF) based on equivalent linearization. RC buildings are simplified into a single-degree-of-freedom (SDOF) model. Seismic response of this SDOF model representing the RC building, when compared to the design target story drift ratio (SDR_{tar}), is used to judge if the building requires to be retrofitted or not. If seismic retrofit is necessary, the required loss stiffness of FVD which corresponds to the necessary amount of damper can be designed without iterative procedure by the proposed method. In addition, a previous study [34] investigated the composite behavior between RC frame and SF in seismic retrofit of RC buildings using BRBs and SFs. The aforementioned study [34] concluded that the required stiffness of BRB or BRB size can be reduced when the composite behavior is considered, while the maximum

* Graduate Student, Dept. of Arch. and Build. Eng., Tokyo Institute of Technology, M. Eng.
** Assist. Prof., Faculty of Civil Engineering, Istanbul Technical University. Dr. Eng.
*** Assist. Prof., Dept. of Arch. and Build. Eng., Tokyo Institute of Technology, Dr. Eng.
**** Prof., Structural & Earthquake Engineering Division, Dept. of Architecture, Istanbul Technical University. Ph. D.
***** Prof., Dept. of Arch. and Build. Eng., Tokyo Institute of Technology, Dr. Eng.

story drift ratio is still within the design target range. Therefore, this study also considers the effect of the composite behavior for the proposed seismic retrofit design. A simplified step-by-step design recommendation is provided. Effectiveness of the proposed design method is demonstrated by performing nonlinear response history analysis (NLRHA) on an example four-story RC school building located in Thailand.

2. RETROFIT DESIGN METHOD

Figs. 1a and 1b show the application layout and the SDOF model representation of the retrofitted RC frame using FVD with SF, respectively. The proposed retrofit design method of RC frame with FVD and SF is introduced in this section.

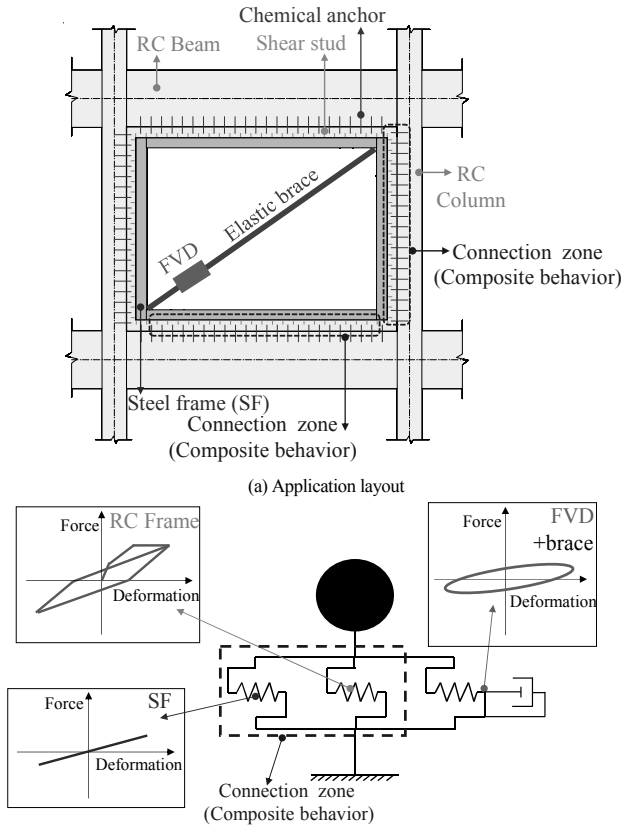

Fig. 1 –Proposed retrofit concept for RC frames

2.1 Simplification of RC building into a SDOF model

As shown in Fig. 2, an existing RC building is simplified from a multi-degree-of-freedom (MDOF) model into an equivalent SDOF model, where H_{eq} is the equivalent height, M_{eq} is the equivalent mass, and K_f is the initial lateral stiffness of the SDOF model of RC building ($SDOF_{RC}$). The H_{eq}, M_{eq}, and K_f can be calculated by Eq. (1), Eq. (2) and Eq. (3), respectively, where m_i is the mass of i^{th} story, u_i is the displacement of i^{th} story, H_i is the height of i^{th} story, and T_f is the fundamental period of the first vibration mode.

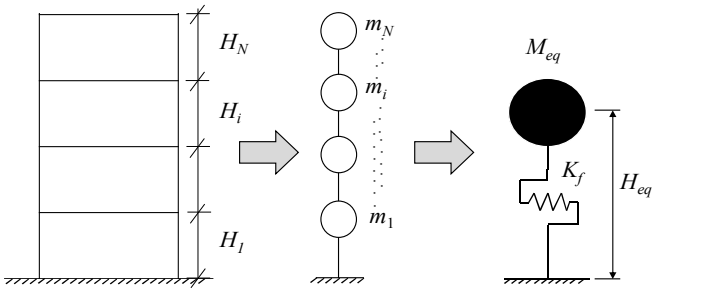

Fig. 2 – Simplification of the RC building into SDOF model

$$H_{eq} = \frac{\sum_{i=1}^{N} m_i \cdot u_i \cdot H_i}{\sum_{i=1}^{N} m_i \cdot u_i} \tag{1}$$

$$M_{eq} = \frac{\left(\sum_{i=1}^{N} m_i \cdot u_i\right)^2}{\sum_{i=1}^{N} m_i \cdot u_i^2} \tag{2}$$

$$K_f = \left(\frac{2\pi}{T_f}\right)^2 M_{eq} \tag{3}$$

Fig. 3 shows the assumed hysteretic response model of $SDOF_{RC}$ at the pre-yielding (cracked, $\mu_c<\mu_f \leq 1$) and post yielding (yielding, $1<\mu_f$) stages [35]. The secant stiffness of the $SDOF_{RC}$ (K_{fu}) is pK_f, where p is the stiffness reduction coefficient determined by Eq. (4). Here, α_1 is the pre-yield stiffness ratio, μ_c is the ratio of lateral crack deformation (δ_{fc}) to lateral yield deformation (δ_{fy}), and μ_f is the ductility ratio (δ_{tar} / δ_{fy}). E_f and E_{fe} are hysteretic and elastic strain energies of the $SDOF_{RC}$, respectively. Q_{fc}, Q_{fy}, and Q_f are the lateral force at the crack, yield, and target deformation stages, respectively. Hysteretic energy (E_f) is given in Eq. (5). The unloading stiffness (K_{ul}) is defined according to the Takeda degrading tri-linear model for the cracking and yielding stages, where the unloading stiffness degradation parameter λ is assumed to be 0.4 [36].

$$\begin{aligned} p &= \frac{\mu_c + \alpha_1(\mu_f - \mu_c)}{\mu_f} \quad \text{for} \quad (\mu_c < \mu_f \leq 1) \\ p &= \frac{\mu_c + \alpha_1(1 - \mu_c)}{\mu_f} \quad \text{for} \quad (1 < \mu_f) \end{aligned} \tag{4}$$

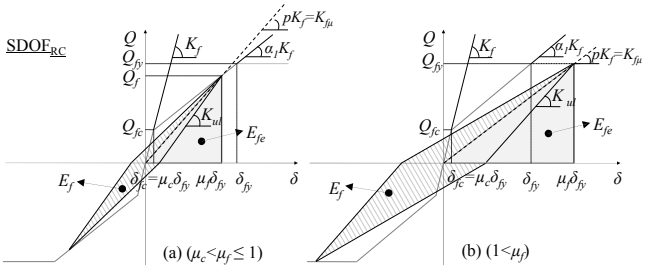

Fig. 3 – Hysteretic loop models and parameters used for $SDOF_{RC}$

$$E_f = 2pK_f(\mu_f\delta_{fy})^2 \cdot \frac{(1-p)\cdot\mu_c}{\mu_c + p\mu_f} \quad \text{for} \quad (\mu_c < \mu_f \le 1)$$
$$E_f = 2pK_f(\mu_f\delta_{fy})^2 \cdot \frac{p\mu_f - p(1+\mu_c)\mu_f^{\lambda} + \mu_c}{\mu_c + p\mu_f} \quad \text{for} \quad (1 < \mu_f) \tag{5}$$

Symbols A_{f1} and A_{f2} are introduced to simplify equations in the next steps.

$$A_{f1} = \frac{(1-p)\cdot\mu_c}{\mu_c + p\mu_f} \quad \text{for} \quad (\mu_c < \mu_f \le 1)$$
$$A_{f2} = \frac{p\mu_f - p(1-\mu_c)\mu_f^{\lambda} + \mu_c}{\mu_c + p\mu_f} \quad \text{for} \quad (1 < \mu_f) \tag{6}$$

2.2 Damper distribution for RC building retrofit

This section introduces assumptions to obtain damper distribution equations for retrofitting RC buildings with FVDs.

2.2.1 Required ratio of FVD loss stiffness (K''_a) to frame stiffness (K_f)

Hysteretic response of FVD is considered in the SDOF model, which is parallel to the $SDOF_{RC}$, as shown in Fig. 1. Fig. 4a shows the retrofitted model, where the FVD is modelled with serially connected spring representing the braces. An elliptic force-deformation relation is assumed for the FVD, while the supplemental SF is assumed to remain elastic within the design target deformation range (δ_{tar}), as indicated in Fig. 4b.

The equation to evaluate the required ratio of loss stiffness of the FVD to frame stiffness (K''_a / K_f) is proposed based on the following assumptions:

(1) Hysteretic energy of the FVD (E_d) is obtained by Eq. (7), where K''_a is loss stiffness of FVD.

$$E_d = \pi K''_a\left(\mu_f\delta_{fy}\right)^2 \tag{7}$$

(2) Storage (K'_a) and loss stiffness of the viscous damper can be calculated by Eq. (8) and Eq. (9), respectively, where K_b is the elastic brace stiffness, C_d is the damping coefficient of FVD, and ω is the circular frequency of bare RC frame, which is calculated by $\omega = 2\pi/T_f$. η_a is the loss factor of the brace+damper subassembly and it can be obtained by Eq. (10).

$$K'_a = \frac{C_d^2K_b\omega^2}{K_b^2 + C_d^2\omega^2} \tag{8}$$

$$K''_a = \frac{C_dK_b^2\omega}{K_b^2 + C_d^2\omega^2} \tag{9}$$

$$\eta_a = \frac{K''_a}{K'_a} = \frac{K_b}{C_d\omega} \tag{10}$$

(3) An equivalent hysteretic damping ratio of the retrofit structure (ξ'_{eq}) can be calculated using Eq. (11), where $E_{\Sigma fe}$ is the total strain energy of the retrofitted structure, and the initial damping ratio of the RC frame is assumed to be $\xi_{f0} = 0.03$.

$$\xi'_{eq} = \xi_{f0} + \frac{E_f + E_d}{4\pi E_{\Sigma fe}} \tag{11}$$

(4) As the displacement ductility in each cycle varies when subjected to earthquake excitation, Newmark and Rosenblueth [37] and Kasai et al. [33] proposed an average damping concept as given in Eq. (12). Average equivalent hysteretic damping ratio of the retrofit structure (ξ_{eq}) is assumed constant at all displacement amplitudes, and ξ_{eq} can be calculated by Eq. (13) in order to simplify the design procedure. To evaluate equivalent damping of $SDOF_{RC}$ ($\xi_{f\mu}$), E_d is substituted by zero, and the E_{fe} considers only the RC frame part, where the damping reduction factor (C_r) is assumed to be 0.7 [38].

$$\xi_{eq} = \xi_{f0} + \frac{1}{\mu_{tar}}\int_1^{\mu_{tar}}\left(\xi'_{eq} - \xi_{f0}\right)d\mu \tag{12}$$

$$\xi_{eq} = \xi_{f0} + C_r\left(\frac{E_f + E_d}{4\pi E_{fe}}\right) \tag{13}$$

(5) The damping response reduction factor (R) was proposed in [33] and given in Eq. (14). In this study, a=25 is used for actual earthquake records.

$$R = \sqrt{\frac{1 + a\xi_{f\mu}}{1 + a\xi_{eq}}} \tag{14}$$

(6) The target story drift at each story ($\theta_{tar,i}$) is assumed constant ($\theta_{tar,i} = \theta_{tar}$).

Based on these assumptions (1) through (6) and using A_{f1} and A_{f2} from Eq. (6), the ratio of the damper to frame stiffness (K''_a / K_f) or r_{f1} for the pre-yielding ($\mu_c < \mu_f \le 1$) and r_{f2} for post yielding stage (yielding, $1 < \mu_f$) can be obtained by Eq. (15), where $\theta_{f\mu}$ is story drift ratio of $SDOF_{RC}$ and θ_{tar} is target story drift ratio.

$$r_{f1} = \frac{K''_a}{K_f} = \frac{p\left(\left(\frac{\theta_{f\mu}}{\theta_{tar}}\right)^2 - 1\right)\cdot\left(1 + a\left(\xi_{f0} + \frac{C_rA_{f1}}{\pi}\right)\right)\cdot\eta_a}{1 + a\xi_{f0} + \frac{a\eta_aC_r}{2\pi}} \quad \text{for} \quad (\mu_c < \mu_f \le 1)$$
$$r_{f2} = \frac{K''_a}{K_f} = \frac{p\left(\left(\frac{\theta_{f\mu}}{\theta_{tar}}\right)^2 - 1\right)\cdot\left(1 + a\left(\xi_{f0} + \frac{C_rA_{f2}}{\pi}\right)\right)\cdot\eta_a}{1 + a\xi_{f0} + \frac{a\eta_aC_r}{2\pi}} \quad \text{for} \quad (1 < \mu_f) \tag{15}$$

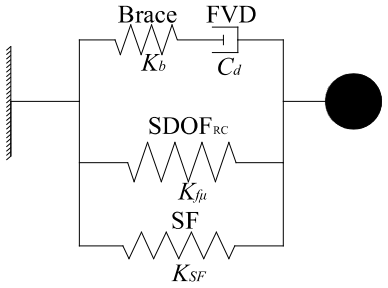

(a) Retrofitted model

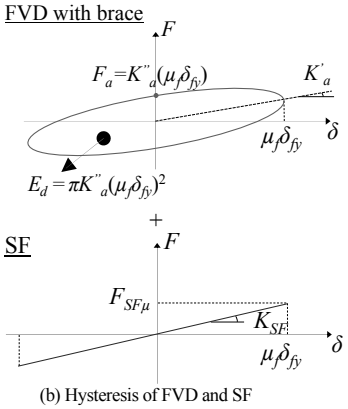

(b) Hysteresis of FVD and SF

Fig. 4 –Retrofitted system modelling assumptions

2.2.2 Required loss stiffness of the FVD ($K''_{a,i}$)

The required loss stiffness of FVD at i^{th} story ($K''_{a,i}$) which corresponds to the necessary amount of damper given in Eq. (16) can be obtained with the following assumptions:

(1) The lateral force for the i^{th} story (Q_i) can be calculated based on either A_i distribution described in the Japanese seismic design [38] or the ASCE-SEI7 specifications [39].

(2) Under the lateral force distribution, maximum story drift (θ_{max}) at each story is equal to θ_{tar}.

(3) The RC frame (μ_{fi}) ductilities at θ_{max} are the same in all stories.

$$K''_{a,i} = \frac{Q_i}{H_i}\frac{\sum_{i=1}^{N}\left(K_{f\mu i}H_i^2\right)}{\sum_{i=1}^{N}\left(Q_iH_i\right)}\left(\eta_a + \frac{\mu_f}{\alpha_1(\mu_f-\mu_c)+\mu_c}\cdot r_{f1}\right) - \eta_a K_{f\mu i} \quad \text{for} \quad (\mu_c < \mu_f \le 1) \tag{16}$$

$$K''_{a,i} = \frac{Q_i}{H_i}\frac{\sum_{i=1}^{N}\left(K_{f\mu i}H_i^2\right)}{\sum_{i=1}^{N}\left(Q_iH_i\right)}\left(\eta_a + \frac{\mu_f}{\alpha_1(1-\mu_c)+\mu_c}\cdot r_{f2}\right) - \eta_a K_{f\mu i} \quad \text{for} \quad (1 < \mu_f)$$

3. EFFECT OF COMPOSITE BEHAVIOR BETWEEN RC FRAME AND ELASTIC STEEL FRAME

Impact of composite behavior between RC frame and SF for seismic retrofit of RC buildings with BRB has been investigated through a parametrical study in [34]. Experimental setup [40] and numerical models [34] of the previous studies are briefly introduced in this section. The study presented in [34] concluded that the required BRB stiffness which corresponds to damper demand could be reduced when the composite behavior is considered. Note that the maximum story drift ratio is still successfully achieved within the target story drift ratio range with a reduced amount of dampers. The current work being an extension of previous work implements a similar composite behavior contribution to reduce the required amount of FVDs.

3.1 Experimental setup

This section briefly introduces a series of RC frame tests with and without SFs. Composite behavior in question is provided by the connection zone between RC frame and SF. The specimens were tested under quasi-static reversed cyclic loading and an analytical method to evaluate the composite behavior has been developed using the experimental results [40].

Fig. 5a shows the test setup of the RC frame specimen retrofitted with SF only (denoted as the "RS specimen"). Fig. 5b shows the details of the RS specimen and cross-sections of the RC beams and columns. Compressive strength of concrete used (σ_c) is 20 MPa, and the yield strength of the steel rebar is taken to be 420 MPa. A load transfer beam on the top of RC column is connected to the strong floor with high-strength rods. There is a hydraulic cylinder between the transfer beam and the column that applies the compression force on the column. Gravity load from the upper stories and applying a constant vertical load of 250 kN on top of each column, which is equivalent to 15% of the column axial force capacity.

Fig. 5b also illustrates the connection zone details between the RC frame and SF. Steel studs (13 mm diameter) were welded to the web of the SF, and chemical anchors (16 mm diameter) were embedded into the RC frame member to a depth of 145 mm. The steel studs and chemical anchors were uniformly distributed with a spacing of 150 mm. Ladder stirrups were placed for cracking control and the space between the SF member and RC frame was then filled with high strength mortar (80 MPa compressive strength).

Cyclic performance of the bare RC frame (denoted as the "R specimen") was compared to that of RS specimen in order to investigate the effect of composite behavior between the RC frame and SF. Test results have shown that SF remained elastic up to 0.67% story drift ratio (1/150 rad.). The test results indicated that because of the composite behavior, the combined lateral stiffness of the RC frame and SF is higher than the simple sum of RC frame and SF stiffnesses [40].

(a) RS specimen

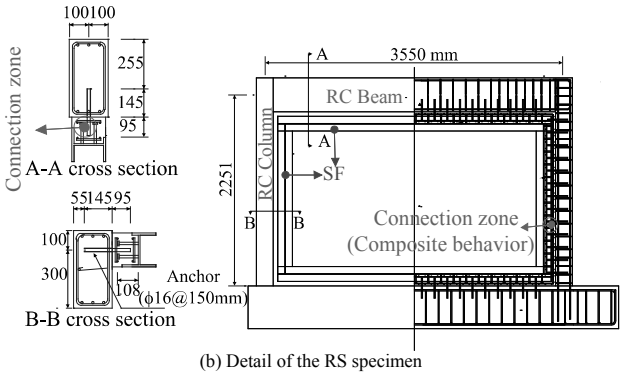

(b) Detail of the RS specimen

Fig. 5 –RS specimen [40]

3.2 Calibration of numerical models

This section briefly introduces the calibration of numerical models constructed using ETABS [41], as shown in Fig. 6. The ETABS models were used to investigate the seismic performance of the retrofitted structure and composite behavior between the RC frame and SF in a previous study [34]. The numerical models are calibrated by using the aforementioned cyclic loading tests [40].

Cyclic nonlinear pushover analyses were performed on the numerical models. A multi-linear plastic (MLP) link, as shown in Fig. 6, was used to represent the connection zone between the RC frame and SF. Fig. 7 compares the base shear to story drift response of the numerical analyses [34] and test results [40]. The slight difference in the initial stiffness and strength may be attributed to the simplified material modeling and the complex nonlinear behavior of the connection zone. The effect of composite behavior is clearly reflected by these models and the accuracy is sufficient for the purposes of this investigation [34].

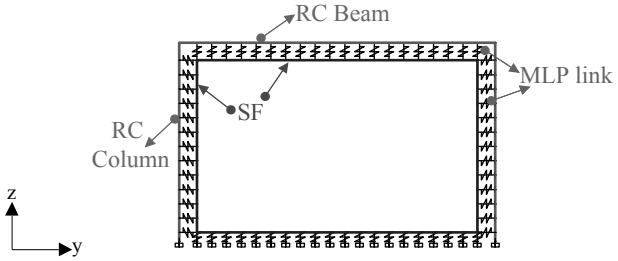

Fig. 6 – Numerical model [34]

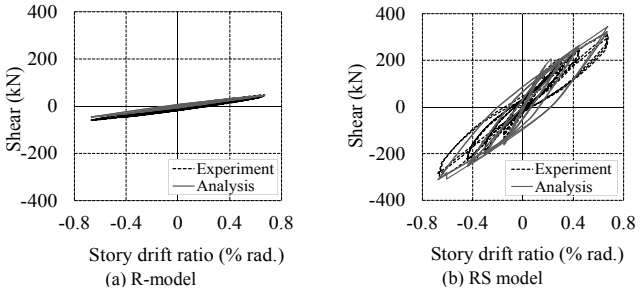

Fig. 7 – Comparison of shear force and story drift ratio from experiments and analyses. [34]

The study presented in [34] obtained a linear-like relationship between $\gamma_{cf,i}$ and $\gamma_{cp,i}$ for four-story RC building. Here, $\gamma_{cf,i}$ is a fully composite stiffness amplification ratio at i^{th} story, expressing the fully composite stiffness relative to the non-composite total stiffness of the RC frame and SF. Also, $\gamma_{cp,i}$ is a partially composite stiffness amplification ratio at i^{th} story, expressing the actual composite stiffness obtained from pushover analysis relative to the non-composite total stiffness of the RC frame and SF. The composite behavior is estimated by the empirical equations, which include non-linear behavior from concrete members (cracking), shear studs (yielding) and other effects such as cracking of the grout, except the elastic steel frame until the target story drift.

Based on the analysis results [34], the relationship of $\gamma_{cf,i}$ and $\gamma_{cp,i}$ is expressed as $\gamma_{cp,1} = 0.45\ \gamma_{cf,1}+0.55$ for the 1st story and $\gamma_{cp,i} = 0.25\ \gamma_{cf,i} + 0.75$ for upper stories. In addition, the key parameters obtained from the single-story RS specimen test was used to confirm the relationship. Based on these previous results, this study applies the relationship to reduce the required loss stiffness of the FVD including the composite behavior ($K''_{ac,i}$) as shown in Eq. (17), where $K_{RC,i}$ and $K_{SF,i}$ are lateral stiffness of RC frame and SF within the retrofit bay i^{th} story, respectively. When there is no composite behavior between RC frame and SF (RC frame and SF act independently), the values of $\gamma_{cp,1}$ and $\gamma_{cp,i}$ becomes 1 as the $K''_{ac,i}$ will be equal to $K''_{a,i}$. Furthermore, the composite behavior is the highest value when the ratio of $K_{SF,i}$ / $K_{RC,i}$ is between 0.50 and 0.75. Therefore, this study uses this benefit to design the SF size.

$$
\begin{aligned}
K''_{ac,1} &= K''_{a,1} - \left(\gamma_{cp,1} - 1\right)\left(K_{RC,1} + K_{SF,1}\right) \\
&= K''_{a,1} - 0.45\left(\gamma_{cf,1} - 1\right)\left(K_{RC,1} + K_{SF,1}\right) \geq 0 \\
K''_{ac,i} &= K''_{a,i} - \left(\gamma_{cp,i} - 1\right)\left(K_{RC,i} + K_{SF,i}\right) \\
&= K''_{a,i} - 0.25\left(\gamma_{cf,i} - 1\right)\left(K_{RC,i} + K_{SF,i}\right) \geq 0 \quad \text{for } i > 1
\end{aligned}
\tag{17}
$$

The recommended retrofit design is summarized in the following steps:

1. Perform the pushover analysis to obtain story stiffnesses of existing RC building ($K_{f,i}$).
2. Compare θ_{fu} with θ_{tar}. If θ_{fu} exceeds θ_{tar}, the building requires a seismic retrofit.
3. Simplify the RC building to a $SDOF_{RC}$ and calculate E_f by using Eq. (1) through Eq. (5).
4. Calculate K''_a / K_f from Eq. (15).
5. Calculate $K''_{a,i}$ from Eq. (16).
6. Select the SF section by choosing ratio of $K_{SF,i}$ / $K_{RC,i}$ between 0.50 and 0.75.
7. Calculate the $K''_{ac,i}$ from Eq. (17) that satisfies the required loss stiffness, considering the composite behavior between the RC frame and SF.

4 . VALIDATION OF THE PROPOSED RETROFIT DESIGN METHOD

This section validates the effectiveness of the proposed seismic retrofitting method for a four-story RC building by using a combination of FVD and SF.

4.1 Target building and seismic region

A typical four-story RC school building is chosen as an example building in this study. The example RC building is located in Chiang Rai province, which is the northernmost province of Thailand. Fig. 8a shows the structural elevation of the four-story RC school building. Fig. 8b presents the cross-sectional details of the RC columns. Fig. 8c shows the structural plan, and Fig. 8d presents the cross-sectional details of the RC beams. The compressive strength of concrete is 24 MPa, and the yield stress of the rebars is 300 MPa. The masses are 184 tons in the 1st to 3rd stories and 171 tons in the 4th story, as shown in Table 1. Also, Table 1 shows the lateral force distribution of the RC building. The concrete slab is typically 100 mm thick in each story. Based on the modal analysis, the first to the third mode periods are 1.249 sec (translation in the longitudinal direction), 0.871 sec (torsional deformation), and 0.830 sec (translation in the transverse direction), respectively.

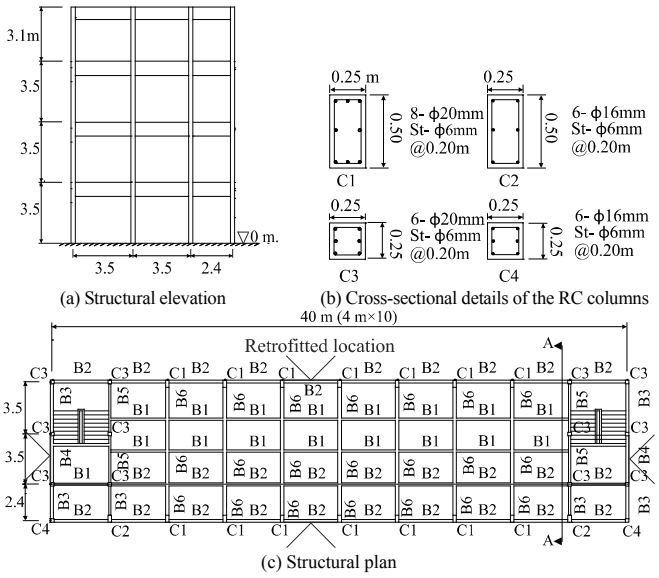

(a) Structural elevation (b) Cross-sectional details of the RC columns

(c) Structural plan

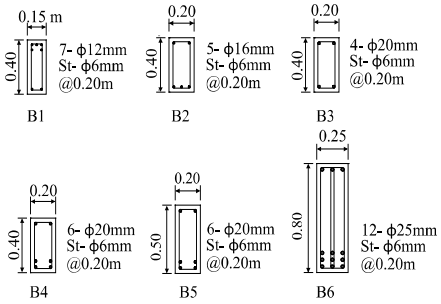

(d) Cross-sectional details of the RC beams

Fig. 8 –Details of the four-story RC school building in Thailand

Fig. 9a presents the maximum considered event (MCE) level acceleration response spectrum, which is the 1.5 times of design acceleration level, corresponding to a damping ratio of 5% in Thailand (Chiang Rai province) [42], where S_{DS} is the design spectral acceleration when the period is 0.2 sec and S_{D1} is the design spectral acceleration when the period is 1.0 sec. Fig. 9b shows the corresponding displacement response spectrum accordingly. The target story drift ratio (θ_{tar}) in this study is limited to 1/200 rad. (0.5% rad.).

The four-story RC school building is converted to a $SDOF_{RC}$ model, as shown in Table 2, with the H_{eq} = 10 m (73.5% of building height), and the M_{eq} = 577 tons (80% of the total mass). Lateral stiffnesses of the $SDOF_{RC}$ model in the longitudinal ($K_{f,l}$) and transverse ($K_{f,t}$) directions are 14.6 and 33.1 kN/mm, respectively. Based on the displacement spectrum (Fig. 9b), the spectral displacements of the $SDOF_{RC}$ model are 111 and 74 mm in the longitudinal ($\delta_{d,l}$) and transverse ($\delta_{d,t}$) directions, respectively. As a result, the maximum story drift ratio (SDR_{max}) of the building in the longitudinal and transverse directions before seismic retrofit is 1.11% ($=\delta_{d,l}/H_{eq}$) and 0.74% rad. ($\delta_{d,t}/H_{eq}$), respectively. Therefore, both directions require retrofitting. Potential retrofit locations are shown in Fig. 8c.

Table 1 Mass and lateral force distribution of the RC building

Bare RC Building (Before retrofit)		
Story	m_i (tons)	Q_i (kN)
4	171	180.5
3	184	302.0
2	184	371.6
1	184	398.4

Table 2 Design results of simplification of the RC building to SDOF

H_{eq} (m)	M_{eq} (tons)	$K_{f,l}$ (kN/mm)	$K_{f,t}$ (kN/mm)
10	577	14.6	33.1

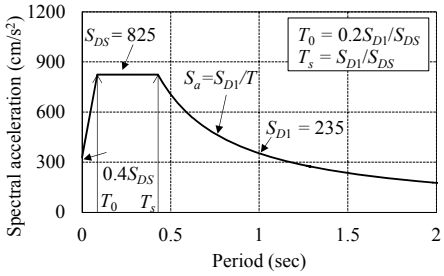

(a) Acceleration

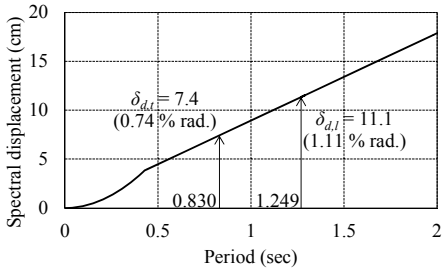

(b) Displacement

Fig. 9 –Design spectra of Chiang Rai province in Thailand (MCE level)

4.2 Retrofit design example

Effectiveness of the proposed retrofit method with FVD is validated according to the design target story drift ratio and also by comparing it to the previously proposed retrofit method implementing BRBs.

Table 3 and Table 4 show the retrofit design results of the example four-story RC school building, where the retrofit is based on the CD method using BRBs [31-32] for longitudinal and transverse directions, respectively. The elastic story stiffness of RC building in the i^{th} story (K_{fi}) is obtained by performing pushover analysis. $K_{BRB,i}$, $\delta_{BRBy,i}$ and $F_{BRB,i}$ are required lateral stiffness, lateral yield deformation, and yield strength of BRB without composite behavior at i^{th} story, respectively. The composite behavior for the retrofitted case with BRBs is considered based on [34]. $K_{BRBC,i}$ and $F_{BRBC,i}$ are required lateral stiffness and yield strength of BRBs including the composite behavior between RC frame and SF at i^{th} story, respectively.

Table 3 Retrofit design results using BRBs (longitudinal direction)

Story	Before retrofit	Buckling-restrained brace				
		without composite behavior (CD method)			with composite behavior	
	$K_{f,i}$ (kN/mm)	$K_{BRB,i}$ (kN/mm)	$\delta_{BRBy,i}$ (mm)	$F_{BRB,i}$ (kN)	$K_{BRBC,i}$ (kN/mm)	$F_{BRBC,i}$ (kN)
	by pushover analysis	[31-32]			[34]	
4th	39.6	16.8	4.8	80.6	6.5	31.0
3rd	32.2	100.1	5.3	530.5	74.2	393.2
2nd	32.1	144.7	5.3	766.9	118.8	629.5
1st	45.3	124.0	5.3	657.2	77.3	409.9

Table 4 Retrofit design results using BRBs (transverse direction)

Story	Before retrofit	Buckling-restrained brace				
		without composite behavior (CD method)			with composite behavior	
	$K_{f,i}$ (kN/mm)	$K_{BRB,i}$ (kN/mm)	$\delta_{BRBy,i}$ (mm)	$F_{BRB,i}$ (kN)	$K_{BRBC,i}$ (kN/mm)	$F_{BRBC,i}$ (kN)
	by pushover analysis	[31-32]			[34]	
4th	74.8	-	-	-	-	-
3rd	70.2	79.1	5.3	415.3	60.3	316.8
2nd	74.5	131.1	5.3	688.3	102.7	539.1
1st	106.6	64.6	5.3	339.2	31.8	167.2

Table 5 and Table 6 present the retrofit design results of the example four-story RC school building with FVDs for longitudinal and transverse directions, respectively. The required ratio of loss stiffness of the FVD (K''_a) to frame (K_f), is obtained to be 0.73 for longitudinal direction and 0.22 for transverse direction. These results are obtained by Eq. (15), assuming loss ratio, η_a is equal to 1. It should be noted that both displacement and base shear are effectively reduced when the amount of damper is designed in an optimal range. The required loss stiffness of FVD on the i^{th} story ($K''_{a,i}$) without considering the composite behavior is obtained by Eq. (16). The design results show that FVDs are not required for the 4th story in either plan direction, while BRBs were required for the 4th story for only longitudinal direction.

Moreover, the required loss stiffness of FVDs on the i^{th} story ($K''_{ac,i}$) including the composite behavior is obtained by Eq. (17). Lateral stiffness of each RC frame within the retrofit bay in longitudinal ($K_{RC,l}$) and transverse ($K_{RC,t}$) directions are 3.2 and 3.65 kN/mm, respectively. SF section H-200×200×8×12 is selected for retrofit in both directions. Lateral stiffness of SF within the retrofit bay in longitudinal ($K_{SF,l}$) and transverse ($K_{SF,t}$) directions are 2.3 and 2.5 kN/mm, respectively. The design result shows that the FVDs are eliminated on the 1st story in transverse direction when the composite behavior is considered in the retrofit design. The proposed damper retrofit designs will be confirmed using NLRHA in the following sections.

Table 5 FVDs retrofit design results (longitudinal direction)

Story	Fluid Viscous damper brace					
	without composite behavior			with composite behavior		
	$K''_{a,i}$ (kN/mm)	$C_{d,i}$ (kN·sec/mm)	$F_{a,i}$ (kN)	$K''_{ac,i}$ (kN/mm)	$C_{dc,i}$ (kN·sec/mm)	$F_{ac,i}$ (kN)
	[Eq.16]			[Eq.17]		
4th	-	-	-	-	-	-
3rd	31.5	12.5	550.5	22.4	8.9	392.0
2nd	60.3	24.0	1055.3	51.2	20.4	896.0
1st	33.5	13.3	586.1	17.2	6.8	301.0

Table 6 FVDs retrofit design results (transverse direction)

Story	Fluid Viscous damper brace					
	without composite behavior			with composite behavior		
	$K''_{a,i}$ (kN/mm)	$C_{d,i}$ (kN·sec/mm)	$F_{a,i}$ (kN)	$K''_{ac,i}$ (kN/mm)	$C_{dc,i}$ (kN·sec/mm)	$F_{ac,i}$ (kN)
	[Eq.16]			[Eq.17]		
4th	-	-	-	-	-	-
3rd	12.2	3.2	212.8	2.8	0.7	49.0
2nd	39.6	10.5	693.5	30.2	8.0	528.5
1st	13.9	3.7	243.4	-	-	-

4.3 Three-dimensional (3-D) numerical model

In this work, numerical models are built in ETABS [41] to confirm the seismic performance of the retrofitted building. The existing RC building model (3D-R) is used as a benchmark. The 3D-R model is constructed based on the numerical model introduced in [34].

Performance of the retrofitted models designed using the proposed retrofit method with braced-viscous dampers (3D-RV) is shown in Fig. 10a.

For modeling the FVDs, a link type of damper-exponential is used [41]. For nonlinear properties, the damping coefficient of FVD ($C_{d,i}$) is assigned to "damping" property, the stiffness of elastic brace ($_\theta K_{b,i}$) is assigned to "stiffness" property while the value of 1.0 is assigned to the "damping exponent" to represent the linearity of viscous damper. η_a is assumed to be 1 in this study for conservative design. It implies that $K_b = C_d\,\omega$ and $K''_a = K'_a$ from the relationship given in Eq 10. When substituting $K_b = C_d\,\omega$ into K'_a equation, the required damping coefficient of FVDs ($C_{d,i}$) can be obtained by $C_{d,i} = 2K''_{a,i}/\omega$, where the circular frequencies of longitudinal and transverse directions are ω_l = 5.03 rad/sec and ω_t = 7.57 rad/sec, respectively. $F_{a,i}$ can be calculated by $K''_{a,i}(\mu_f\,\delta_{fy})$, as shown in Fig 4a. For example, $F_{a,2}$ from $K''_{a,2}(\mu_f\,\delta_{fy})$, where μ_f = 0.5 and δ_{fy} is 1/100 rad × story height. $F_{a,2}$ = 60.3×(0.5×1/100×3500 mm) = 1055.3 kN, as shown in Table 5. results of $C_{d,i}$ and $F_{a,i}$ are shown in Tables 5 and 6 for longitudinal and transverse directions, respectively.

An additional brace is required for practical FVD applications. These braces of FVDs are to be designed to prevent the buckling failure from the axial damper force. In this work, a steel hollow section SHS 150x150x9x9 (SHS-150×9) is selected for bracing each FVD that satisfies $\eta_a \geq 1$. There are two viscous dampers on 1st , 2nd , and 3rd stories. Therefore, the $_\theta F_{a,i}/2$ is an axial force of one viscous damper on i^{th} story. $_\theta K_{b,i}$ is an axial stiffness of brace for one damper. The highest value of $_\theta F_{a,i}/2$ on the 2nd story which is 701.2 kN is used to design the brace's section. Table 7 and Table 8 show the design results of the brace of the viscous damper for the case without composite behavior in longitudinal and transverse directions, respectively. The elastic braces used for both cases have the same size in each direction. The configuration of the braced viscous damper is shown in Figure 1a.

Furthermore, a retrofitted building with braced-viscous damper and SF including composite behavior (3D-RSCV) is modeled to investigate the effect of the composite behavior, as shown in Fig. 10b. The composite behavior modeling method was presented in [34].

Table 7 Designing braces of viscous damper in longitudinal direction

Story	H_i (mm)	L_i (mm)	$_\theta F_{a,i}/2$ (kN)	SHS section type	$_\theta K_{b,i}$ (kN/mm)
4th	3100	4000	-	-	-
3rd	3500	4000	365.8	SHS 150x150x9x9	183.1
2nd	3500	4000	701.2	SHS 150x150x9x9	183.1
1st	3500	4000	389.4	SHS 150x150x9x9	183.1

Table 8 Designing braces of viscous damper in transverse direction

Story	H_i (mm)	L_i (mm)	$_\theta F_{a,i}/2$ (kN)	SHS section type	$_\theta K_{b,i}$ (kN/mm)
4th	3100	3500	-	-	-
3rd	3500	3500	150.5	SHS 150x150x9x9	196.7
2nd	3500	3500	490.4	SHS 150x150x9x9	196.7
1st	3500	3500	172.1	SHS 150x150x9x9	196.7

NLRHA results of the proposed retrofit with FVDs are compared with the results of the bare RC building, BRB retrofit, and BRB+SF retrofit including composite behavior. The retrofitted model using BRBs only (3D-RB model) was designed based on [31-32]. Moreover, the retrofitted building with BRBs and steel frame including composite behavior (3D-RSCB) was designed based on [34]. The definitions of each three-dimensional model are shown in Table 9.

Table 9 Definition of three-dimensional models

Model name	Definition of three-dimensional models
3D-R	Existing RC building (Bare RC building)
3D-RB	Retrofitted building with BRBs only
3D-RV	Retrofitted building with braced-viscous damper only
3D-RSCB	Retrofitted building with BRBs and SF including composite behavior
3D-RSCV	Retrofitted building with braced-viscous damper and SF including composite behavior

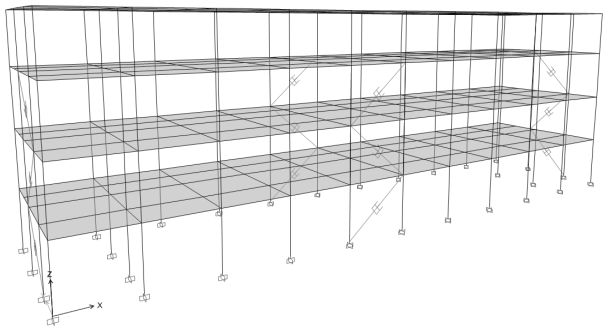

(a) 3D-RV model

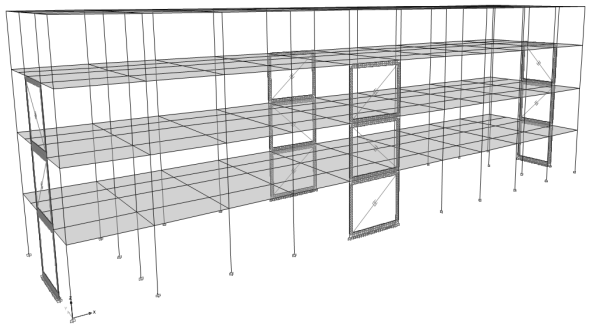

(b) 3D-RSCV model

Fig. 10 –3-D view of the analysis models

4.4 Modal Analyses

Fig. 11a shows the periods of the first three longitudinal translational modes. The conducted modal analyses indicate that the fundamental periods decrease from 1.249 sec (3D-R) to 0.687 sec for the 3D-RB, to 0.614 sec for 3D-RV, to 0.673 for RSCB, and 0.586 for RSCV models.

Fig. 12a shows the periods of the first three transverse translational modes. The modal analysis indicates that the fundamental periods decrease from 0.830 sec (3D-R) to 0.645 sec for the 3D-RB, to 0.588 sec for 3D-RV, to 0.619 for RSCB, and 0.610 for RSCV models.

Furthermore, the modal analysis, as shown in Fig. 11b and Fig. 12b, indicates that the translation mode shape of the retrofitted buildings changes slightly when compared to the bare RC frame (3D-R) in both directions.

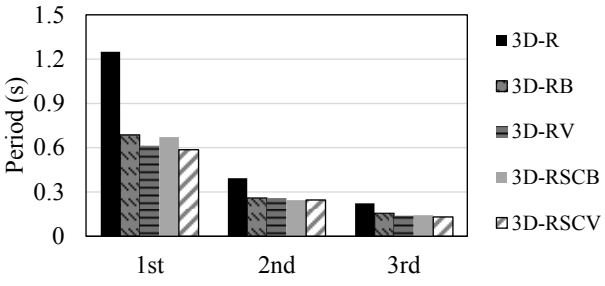

(a) Vibration period

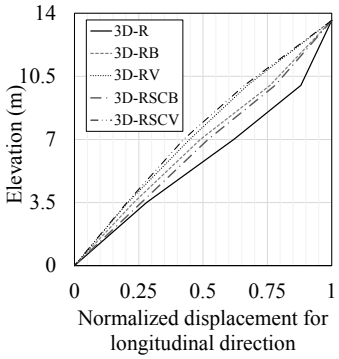

(b) Translation mode shape

Fig. 11 –Modal analysis results for the longitudinal direction

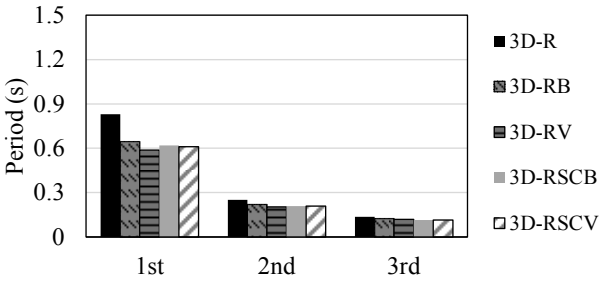

(a) Vibration period

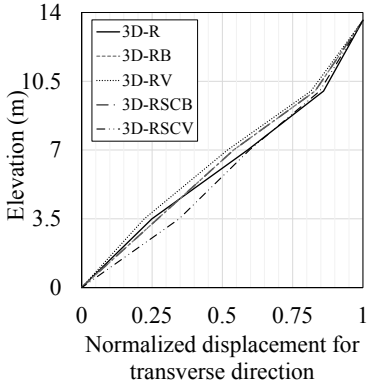

(b) Translation mode shape

Fig. 12 –Modal analysis results for the transverse direction

4.5 Nonlinear response history analyses (NLRHA)

Nonlinear response history analyses (NLRHA) are performed for 3D-R, 3D-RB, 3D-RV, 3D-RSCB, and 3D-RSCV models using a suite of eleven ground motions to investigate the seismic response and verify the effectiveness of the proposed retrofit design method. Seismic performance of each model is evaluated using the average and average plus one standard

deviation (SD) of the analysis results for the different ground motion records.

4.5.1 Ground motions for NLRHA

A suite of eleven scaled single component records is selected from the PEER NGA2 ground motion database 2 [43]. Fig. 13 shows the response spectra of the scaled ground motions. The detailed information of each ground motion is shown in [34]. The selected spectra have been scaled to fit the MCE level.

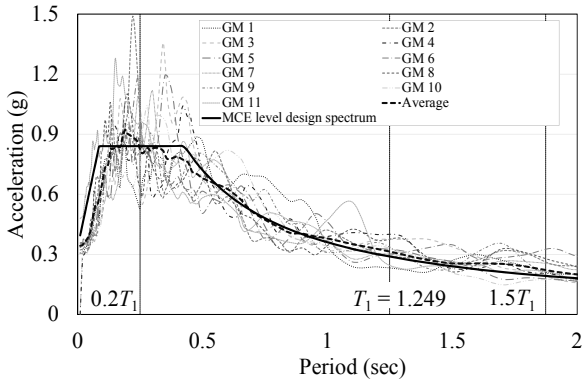

Fig. 13 –5% damped response spectra of the scaled ground motions and the MCE level design acceleration spectrum

4.5.2 Maximum story drift ratio

Maximum inter-story drift ratio (SDR_{max}) of the bare RC building and retrofitted buildings are shown in Fig. 14 and Fig. 15, for longitudinal and transverse directions, respectively. The SDR_{max} results of the retrofitted building with FVDs are compared to the results of bare RC building (3D-R) in Fig. 14a and Fig. 15a, and retrofitted buildings with BRBs to validate the effectiveness of the proposed retrofit method with FVDs.

The NLRHA results indicated that the proposed method could control an average of SDR_{max} of the RV model within the selected SDR_{tar} of 0.5% rad for both directions, as shown in Fig. 14c and Fig. 15c. The results of the proposed method with FVDs show a similar trend to the results of the RB model, as shown in Fig. 14b for longitudinal and Fig. 15b for transverse directions.

Moreover, the NLRHA results show that the SDR_{max} of the RSCV model is within 0.5% rad for both directions, as shown in Fig. 14e and Fig. 15e. These results also show a similar trend to the results obtained for the RSCB model, as shown in Fig. 14d and Fig. 15d for longitudinal and transverse directions, respectively. It implies that including the composite behavior can reduce the required loss stiffness ($K''_{a,i}$) of FVDs, which could lead to more economical solutions.

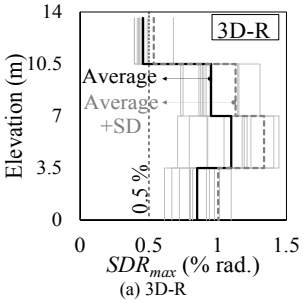

(a) 3D-R

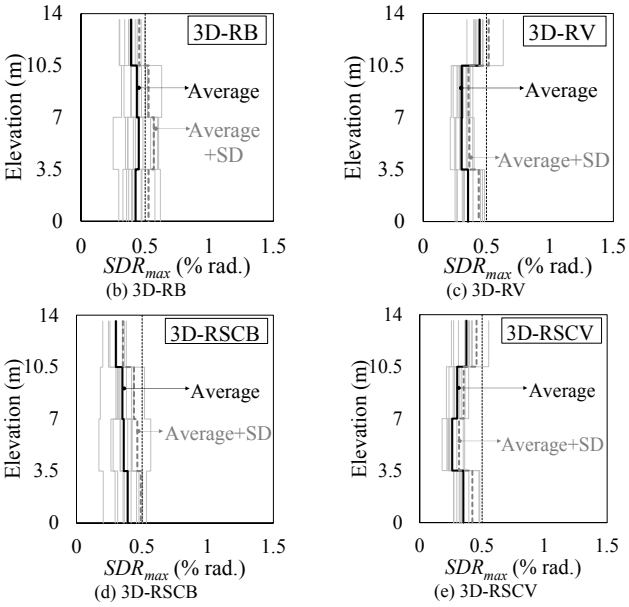

(b) 3D-RB (c) 3D-RV (d) 3D-RSCB (e) 3D-RSCV

Fig. 14 – Maximum inter-story drift ratios for longitudinal direction

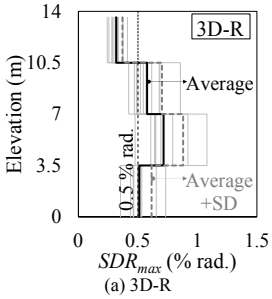

(a) 3D-R

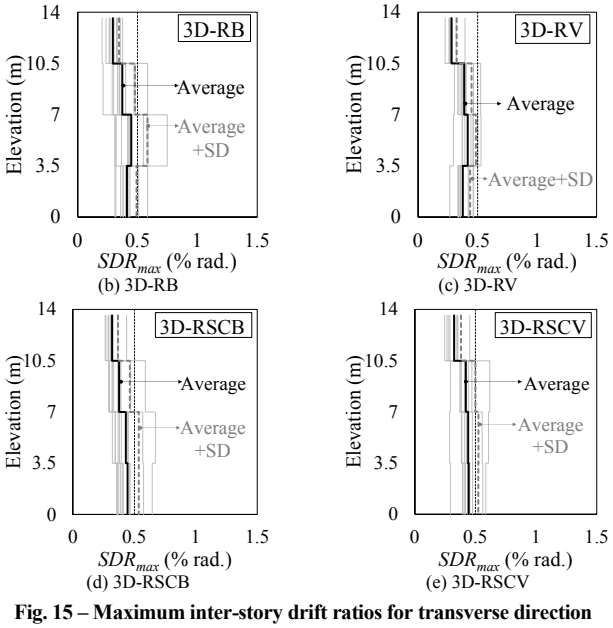

(b) 3D-RB (c) 3D-RV (d) 3D-RSCB (e) 3D-RSCV

Fig. 15 – Maximum inter-story drift ratios for transverse direction

4.5.3 Residual story drift ratio

Residual drifts of buildings should be mitigated during earthquakes to have better overall seismic performance and repairability. The SDR_{re} is closely related to post-earthquake damage assessment [44]. Following an earthquake, repair and demolition losses could be better evaluated with the help of residual drifts. For example, remaining open cracks in brick partition walls because of residual drifts, should be repaired. The SDR_{re} value is

obtained after 60 sec of free vibration at the end of each NLRHA analysis and compared between analysis models to see the effectiveness of the proposed retrofit.

The NLRHA results of each ground motion, the average, and the average plus one standard deviation (SD) values are shown in Fig. 16 for longitudinal direction. The NLRHA results indicate that both retrofits with BRBs and FVDs could limit the SDR_{re} within 0.1%. Meanwhile, the SDR_{re} NLRHA results for transverse direction, as shown in Fig. 17, indicate a similar trend to the longitudinal direction that the SDR_{re} is within 0.1% for the retrofitted buildings. This implies that both structural and nonstructural damage can be mitigated in the retrofitted buildings.

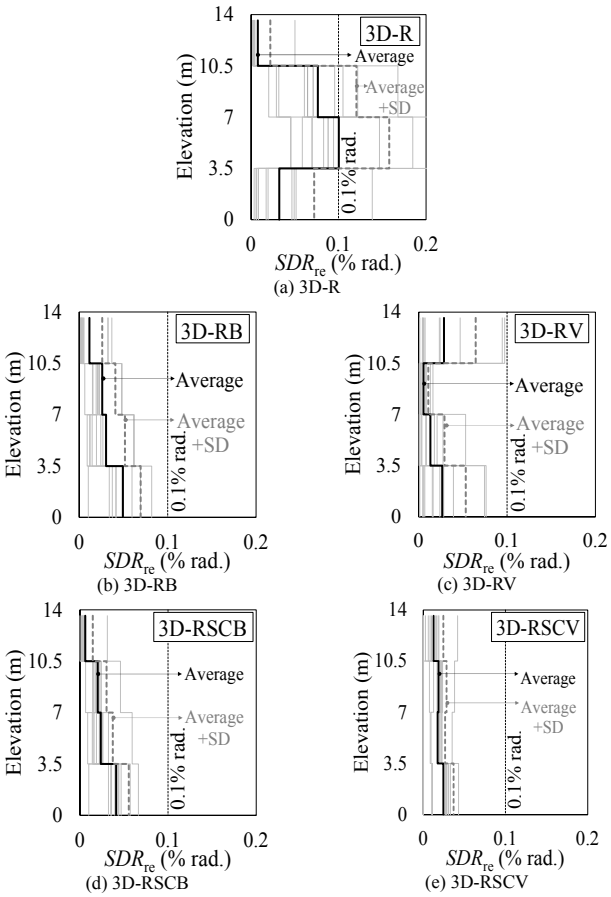

Fig. 16 – Residual story drift ratios for the longitudinal direction

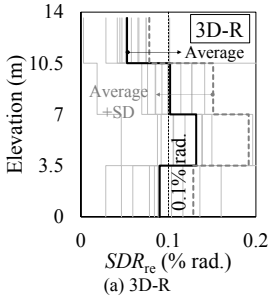

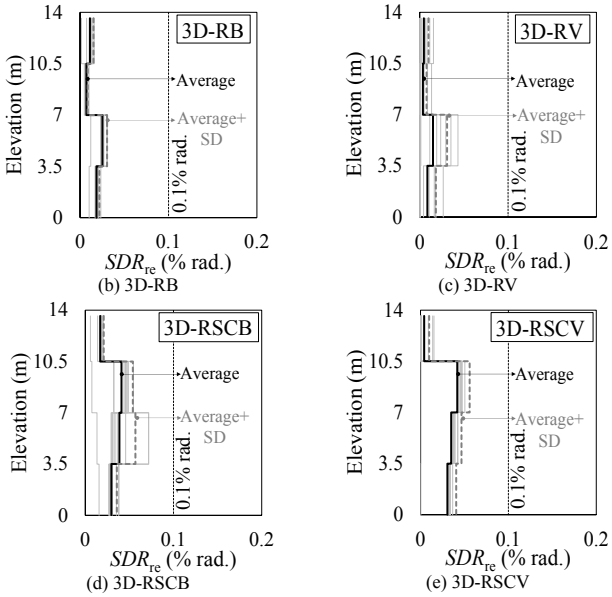

Fig. 17 – Residual story drift ratios for the transverse direction

4.5.4 Maximum roof accelerations

Maximum roof accelerations (A_{max}) in the retrofitted buildings may tend to increase as a result of the additional stiffness introduced by the proposed retrofit schemes, following the acceleration spectrum. However, a reduction in A_{max} is also expected due to the increased/added damping ratio as a natural outcome of energy dissipated by the dampers. Therefore, the final effect was confirmed after NLRHA analyses. Moreover, possible variations in response may be attributed to the different ground motion characteristics. Fig. 18a and Fig. 18b show A_{max} and average of A_{max} from the NLRHA for longitudinal and transverse directions, respectively. Based on the analysis results, A_{max} values obtained for the retrofitted buildings in both directions change slightly when compared to the 3D-R model. As shown in Fig. 18, after the addition of damper retrofit, the average A_{max} has been slightly increased. When the composite behavior is included, the increase is even less significant.

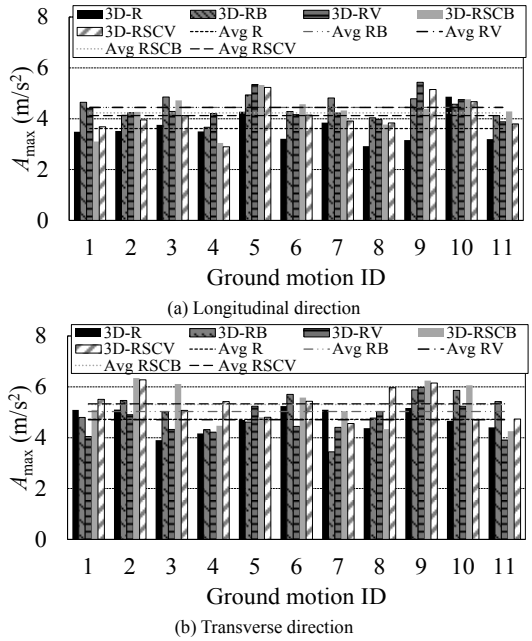

Fig. 18 – Maximum roof acceleration

5. CONCLUSIONS

A seismic retrofit method for RC buildings using fluid viscous dampers (FVDs) implemented with elastic steel frames (SF) based on an equivalent linearization technique is introduced to assign an efficient damper distribution. The proposed method is validated by using the nonlinear response history analyses (NLRHA) on a four-story RC school building located in Thailand. Response parameters of the proposed retrofit method are compared with the numerical results of the existing RC building and CD method with BRBs. Key findings from this work can be drawn as follows:

1) The proposed retrofit method of RC buildings with FVDs and SF can efficiently improve the seismic performance of seismically deficient RC buildings.

2) Effectiveness of the proposed method is compared to the CD method with BRBs. The NLRHA results indicate that the proposed method performs with similar accuracy to the CD method. Also, the average maximum story drift ratio obtained by the proposed retrofit method is within the target range. These results (although limited to the considered buildings in this work) prove the effectiveness of the proposed retrofit method.

3) Composite behavior between the RC frame and SF can be used to reduce the seismic demands of FVDs while the target story drift ratio can still be achieved successfully.

4) The proposed retrofit method with FVDs and SF can reduce the residual story drift ratio values within the widely accepted limit of 0.1%. By this way, both structural and nonstructural damage could be mitigated in the retrofitted buildings while securing the continuous occupancy performance level following a large earthquake.

REFERENCES

1) P Lukkunaprasit, A Ruangrassamee, T Boonyatee, C Chintanapakdee, K Jankaew, N Thanasisathit, and T Chandrangsu. Performance of Structures in the Mw 6 1 Mae Lao Earthquake in Thailand on May 5 2014 and Implications for Future Construction. *Journal of Earthquake Engineering*, pp. 219-242, 2015. 20.
2) T. Ornthammarath and P. Warnitchai. 5 May 2014 MW 6.1 Mae Lao (Northern Thailand) earthquake: interpretations of recorded ground motion and structural damage. *Earthquake Spectra*. pp. 1209–1238, 2016. 32
3) D. Mitchell, R.H. DeVall, M. Saatcioglu, R. Simpson, R. Tinawi, and R. Tremblay. Damage to concrete structures due to the 1994 Northridge earthquake. *Canadian Journal of Civil Engineering*, pp. 361-377, 1995.22.
4) D. Mitchell, R.H. DeVall, K. Kobayashi, R. Tinawi and W.K. Tso. Damage to concrete structures due to the January 17, 1995, Hyogo-ken Nanbu (Kobe) earthquake. *Canadian Journal of Civil Engineering*. pp. 757-770, 1996. 23.
5) K.C Tsai and S.J Hwang. Seismic retrofit program for Taiwan school buildings after 1999 Chi-Chi Earthquake. *14th World Conference on Earthquake Engineering*, 2008.
6) Celik O.C. Holistic Seismic Behavior and Design of Buildings. *FACADE Conference*. pp. 161-173, 2017.
7) Masi A, Chiauzzi L, Santarsiero G, Manfredi V, Biondi S, Spacone E, Gaudio C.D, Ricci P, Manfredi G, Verderame G.M. Seismic response of RC buildings during the Mw 6.0 August 24 2016 Central Italy earthquake the Amatrice case study. Bulletin of *Earthquake Engineering*. pp 5631-5654, 2019. 17.
8) B Binici, G Ozcebe and R Ozcelik. Analysis and design of FRP composites for seismic retrofit of infill walls in reinforced concrete frames. *Composite: Part B*, pp 575-583, 2007. 38.
9) O Ozcan, B Binici and G Ozcebe. Improving seismic performance of deficient reinforced concrete columns using carbon fiber-reinforced polymers, *Engineering Structures*, pp 1632-1646, 2008. 30.
10) Foutch D.A, Hjelmstad K.D, Calderon E.D.V, Gutierrez E.F and Downs R.E. The Mexico earthquake of September 19, 1985: Case studies of seismic strengthening for two buildings in Mexico City. *Earthquake Spectra*. pp. 153–174, 1989. 5.
11) E Canbay, U Ersoy and G Ozcebe. Contribution of reinforced concrete infills to seismic behavior of structural systems. *ACI Structural Journal*. pp. 637–643, 2003. 100.
12) M Badoux and J.O Jirsa. Steel bracing of RC frames for seismic retrofitting. *Journal of Structural Engineering*. pp. 55–74, 1990. 116.
13) H. Fukuyama, S. Sugano. Japanese seismic rehabilitation of concrete buildings after the Hyogoken–Nanbu earthquake. *Cement and Concrete Composites*. pp. 59–79, 2000.
14) M Jara, C Hernandez, R Garcia, F Robles. The Mexico earthquake of September 19, 1985: Typical cases of repair and strengthening of concrete buildings, *Earthquake Spectra*, pp. 175–193, 1989. 5.
15) J. O. Jirsa. Divergent issues in rehabilitation of existing buildings, *Earthquake Spectra*. pp. 95–112, 1994. 10.
16) K.C. Chang, Y.Y. Lin, and C.Y. Chen. Shaking Table Study on Displacement-Based Design for Seismic Retrofit of Existing Buildings Using Nonlinear Viscous Dampers. *Journal of Structural Engineering ASCE*, pp. 671-681, 2008. 134.
17) A. Khampanit, A. Leelataviwat, J. Kochanin, and P. Warnitchai. Energy-based seismic strengthening design of non-ductile reinforced concrete frames using buckling-restrained braces. *Engineering Structures*, 2014, pp. 110-122. 2014. 81.
18) M. Martinez-Rodrigo, M.L. Romero. An optimum retrofit strategy for moment resisting frames with nonlinear viscous dampers for seismic applications. *Engineering Structures*, pp. 913-925. 2003. 25.
19) K. Jinkoo and H. Choi. Displacement-based design of supplemental dampers for seismic retrofit of a framed structure. *Journal of Structural Engineering*, pp. 873-883. 2006. 132.
20) D. Lee and D. P. Taylor. Viscous damper development and future trends. *The structural design of tall buildings*. pp. 311-322. 2001. 10.
21) Y. Zhou, X. Lu, D. Weng, R. Zhang. A practical design method for reinforced concrete structures with viscous dampers. *Engineering Structures*, pp. 187-198, 2012, 39.
22) F. Adachi, S. Yoshitomi, M. Tsuji and I. Takewaki. Nonlinear optimal oil damper design in seismically controlled multi-story building frame. *Soil Dynamics and Earthquake Engineering*. pp. 1-13, 2013. 44.
23) D. De. Domenico, G. Ricciardi, and I. Takewaki. Design strategies of viscous dampers for seismic protection of building structures: A review. *Soil Dynamics and Earthquake Engineering*. pp. 144-165. 2019. 118.
24) Zhang RH, Soong TT. Seismic design of viscoelastic dampers for structural applications. Journal of Structural Engineering, 1992, 118(5): 1375-1392.
25) Fujita K, Moustafa A, Takewaki I. Optimal placement of viscoelastic dampers and supporting members under variable critical excitations. Earthq. Struct, 20 10, 1(1): 43-67.
26) M.J.N. Priestley. Displacement-Based Seismic Assessment of Reinforced Concrete Buildings. *Journal of Earthquake Engineering*, pp. 157-192, 1997. 1:
27) A.K. Chopra and R.K. Goel. Direct Displacement-Based Design: Use of Inelastic vs. Elastic Design Spectra. *Earthquake Spectra*. pp. 47-64. 2001. 17.
28) Y.Y. Lin, M.H. Tsai, J.S. Hwang and K.C. Chang. Direct displacement-based design for building with passive energydissipation systems. *Engineering Structures*, pp. 25–37, 2003. 25:
29) T.J. Maley, T.J. Sullivan, and G.D. Corte. Development of a Displacement-Based Design Method for Steel Dual Systems With Buckling Restrained Braces and Moment-Resisting Frames. *Journal of Earthquake Engineering*, pp. 106-140. 2010. 14(S1).
30) F. Mazza and A. Vulcano. Displacement-based design procedure of damped braces for the seismic retrofitting of r.c. framed buildings. *Bulletin of Earthquake Engineering*. pp. 2121–2143. 2015. 13.
31) K. Fujishita, F. Sutcu, R. Matsui, and T. Takeuchi. Damage distribution based energy-dissipation retrofit method for multi-story RC building in Turkey. *IABSE Symposium Report*, pp. 1-8. 2005. 104.
32) T. Takeuchi, and A. Wada. Buckling-restrained braces and application. The Japan Society of Seismic Isolation.
33) K. Kasai, Y. Fu, and A. Watanabe. Passive Control Systems for Seismic Damage Mitigation. *Journal of Structural Engineering ASCE*, pp. 501-512. 1998 124.

34) P. Saingam, F. Sutcu, Y. Terazawa, K. Fujishita, P.C. Lin, O.C. Celik, and T. Takeuchi. Composite Behavior in RC Buildings Retrofitted using Buckling-Restrained Braces with Elastic Steel Frames. *Engineering Structures*, 2020. 219. 110896.
35) F. Sutcu, T. Takeuchi, and R. Matsui. Seismic retrofitting design method of existing RC buildings with buckling restrained braces, *Journal of Constructional Steel Research*, pp. 304-313. 2014. 101.
36) T. Takeda, M.A. Sozen, and N.N. Nielsen N.N. Reinforced concrete response to simulated earthquakes. *Journal of Structural Engineering*, pp. 2557-2573. 1970. 96.
37) N.M. Newmark and E. Rousenblueth. Fundamentals of Earthquake Engineering. Prentice-Hall 555 Inc., 1971.
38) The Building Center of Japan. The Building Standard Law of Japan on CD-ROM 2016.
39) American Society of Civil Engineers (ASCE) (2016): Minimum Design Loads for Buildings and Other Structures 2016 (ASCE/SEI 7-16).
40) F. Sutcu, A. Bal, K. Fujishita, R. Matsui, O.C. Celik, T. Takeuchi T. Experimental and Analytical Studies of Sub-Standard RC Frames Retrofitted with Buckling-Restrained Braces and Steel Frames. *Bulletin of Earthquake Engineering*, pp. 2389-2410. 2020. 18.
41) Wilson E.L (2015): CSI analysis reference manual for SAP 2000 ETABS, SAFE, and CSI Bridge. Berkeley, Computers & Structures, Inc 2015.
42) Department of Public Works and Town & Country Planning (DPT) (2009): Thailand Seismic Design Code.
43) Pacific Earthquake Engineering Research Center (PEER). PEER NGA Ground motion database, < http://ngawest2.berkeley.edu/site >.